






Air spark-assisted excitation to suppress the self-reversal effect in nanosecond UV laser-induced breakdown spectroscopy

INDRA KARNADI,^{1,*} MARINCAN PARDEDE,² EDWARD HAREFA,^{3,4}
IVAN TANRA,¹ RINDA HEDWIG,⁵  BUDI HARSONO,¹
MARVIN YONATHAN HADIYANTO,¹ TJUNG TJIE LIE,⁶
WEIDONG ZHOU,³  KIICHIRO KAGAWA,^{6,7}
AND KOO HENDRIK KURNIAWAN⁶ 

¹Department of Electrical Engineering, Krida Wacana Christian University, Jakarta, 11470, Indonesia

²Department of Electrical Engineering, University of Pelita Harapan, Tangerang, 15811, Indonesia

³Key Laboratory of Optical Information Detection and Display Technology of Zhejiang, Zhejiang Normal University, Jinhua 321004, China

⁴Currently at: Faculty of Teacher Training and Education, Universitas Nias, Gunungsitoli 22812, Indonesia

⁵Computer Engineering Department, Faculty of Engineering, Bina Nusantara University, Jakarta 11480, Indonesia

⁶Research Center of Maju Makmur Mandiri Foundation, Jakarta 11630, Indonesia

⁷Fukui Science Education Academy, Takagi Chuo 2 Chome, Fukui, 910-0804, Japan

*indra.karnadi@ukrida.ac.id

Abstract: A self-reversal effect in plasma has affected the accuracy of laser-induced breakdown spectroscopy (LIBS). This effect becomes pronounced in a high-density and inhomogeneous plasma, which is commonly generated in UV LIBS due to efficient ablation of the sample by UV irradiation. Here we present a simple method to suppress the self-reversal effect in UV LIBS at atmospheric pressure utilizing an air spark-assisted excitation. We simultaneously generated the air spark and target plasma by adjusting the lens' focal point position relative to the sample surface. The interaction between the air spark's tail and target plasma helps reduce the number of cold ground-state atoms at the periphery of the target plasma. Under this condition, we significantly suppressed the self-reversal effect in the resonance lines of high-concentration aluminum. The time-resolved features show that the emission lines of Al I 394.40 nm and Al I 396.15 nm obtained using the proposed approach are free from self-reversal. These results indicate that the proposed technique can improve the plasma's homogeneity and, therefore, the spectral quality of resonance lines of nanosecond UV LIBS.

© 2023 Optica Publishing Group under the terms of the [Optica Open Access Publishing Agreement](#)

1. Introduction

Over the past decades, laser-induced breakdown spectroscopy (LIBS) has become popular for measuring substances' element content and chemical composition. This technique has been applied in many fields, including mining, environmental monitoring, geology, food safety, nuclear safety, space exploration, etc. [1–7]. It offers several advantages: rapid analysis, real-time, in-situ, less destructive, less sample pre-treatment, and simultaneous multi-elemental analysis. However, the presence of self-absorption and self-reversal effect in the laser-induced plasma, particularly in the high-density and inhomogeneous plasma, often affected the accuracy of LIBS. When the self-absorption effect occurs in plasma, the peak intensity of the emission lines may reduce, thereby breaking a linear relationship between the emission intensity and the analyte concentration. To date, researchers have developed some analytical procedures [8–13], optimized the experimental parameters [14–23], and added additional devices [24–32] to

evaluate or compensate for the effect of self-absorption. The self-absorption effect can be easily evaluated and compensated in the case of homogeneous plasma [11,33]. However, in the case of inhomogeneous plasma, the presence of the self-absorption effect can lead to the self-reversal effect. This self-reversal effect is greatly influenced by the spatial gradient of plasma temperature and electron number density, especially in the outer plasma layer. Because the plasma periphery has a lower temperature than the central plasma region, it will be populated by cold ground state atoms. Besides lower temperature, the plasma periphery has a lower electron density than the inner region. Therefore when a photon emitted by the atom from the hot plasma core travels to the outer plasma region, it can be reabsorbed by a ground-state atom of similar species residing at the plasma periphery. As a result, a narrow absorption line profile, which manifests as a narrow dip, can appear in the emission line. This self-reversal effect is pronounced for a line of a highly concentrated element that has a higher transition rate and ends on a lower energy level that closes to the ground state. Analytically, treating the self-reversed line in inhomogeneous plasma is challenging compared to the self-absorbed line in homogeneous plasma. Therefore the emission line without self-reversal is preferable for quantitative analysis in LIBS.

Recently, several approaches have been proposed to suppress the self-reversal effect in laser-induced plasma. Some researchers have optimized the experimental parameters [17–23] and utilized additional devices [24–31] to improve the plasma's homogeneity and suppress the self-reversal effect in LIBS. However, only a few have discussed the suppression of the self-reversal effect in UV LIBS. It is known that UV laser irradiation can ablate the sample efficiently [34]. However, the plasma produced by UV lasers can have a large inhomogeneity in density and temperature between the core and the periphery, which may induce a self-reversal effect. In their recent work, Urbina et al. [21] investigate the impact of environmental gas on the self-reversal effect in UV LIBS. They found that the self-reversal effect could be reduced if the plasma was surrounded by atomic instead of molecular gas.

In the present work, we demonstrate the suppression of the self-reversal effect in UV LIBS by utilizing an air spark. We simultaneously create the air spark and target plasma by adjusting the lens' focal point on the sample surface. We investigate how the position of the air spark relative to the target plasma can affect the self-reversal effect. We show that the self-reversal effect in UV laser-induced aluminum plasma diminished when the air spark's tail was placed in between the sample surface and the target plasma periphery. We demonstrate the effectiveness of the proposed approach by observing the temporal profile of resonance lines of high-concentration aluminum. Using this technique, we obtained the Al I 394.40 nm ($3s^2(^1S)4s^2S_{1/2} - 3s^2(^1S)3p^2P_{1/2}$) and Al I 396.15 nm ($3s^2(^1S)4s^2S_{1/2} - 3s^2(^1S)3p^2P_{3/2}$) emission lines, free from self-reversal. To our knowledge, this is the first report of utilizing an air spark, generated simultaneously with the target plasma using the same laser, to suppress the self-reversal effect in nanosecond UV LIBS.

2. Experimental setup

Figure 1 displays a schematic diagram of the experimental arrangement used in this work. We conduct the experiments under atmospheric air pressure. A Q-switched Nd: YAG pulsed laser (Quanta Ray model INDI 10), operating at 355 nm, having a pulse duration of 10 ns and a repetition rate of 10 Hz, was employed for plasma generation. The incident laser energy was fixed at 60 mJ. The lens with focal length of 150 mm was used to focus the laser beam. By adjusting the lens' focal point relative to the sample surface, we generate the air spark and target plasma simultaneously. The target used in this study was standard aluminum from Rare Metallic Co. Japan, contains 99.8% aluminum. It was mounted on a 3D-sample stage, which was rotated at 6 rpm to avoid the formation of a deep crater on the target surface during successive laser shots. Spectrums were obtained by averaging ten single-shot data under identical experimental conditions to increase the signal-to-noise ratio. The radiation emitted by the plasma was collected using an optical fiber with a numerical aperture of 0.27. The other end of the optical fiber was

attached to a 5.0 μm wide entrance slit of a 1.0 m Czerny Turner type spectrograph (McPherson model 2061) having a grating of 1800 grooves/mm and a resolution of 0.012 nm at 313.1 nm. The exit slit of the spectrograph was equipped with a time-gated ICCD (Andor iStar intensified CCD, $1,024 \times 256$ pixels, UK) to record the spectra. To synchronize the delay time between the laser pulse and the ICCD, the ICCD was triggered using an output signal from the laser system. An adjustable time gate provided by the ICCD allows the detection of the temporal evolution of plasma emission. In the time-resolved measurement, we set an initial delay of 600 ns to allow the decay of the continuum due to Bremsstrahlung radiation and free-bound electronic transition recombination. Data acquisition and analysis were carried out with a personal computer.

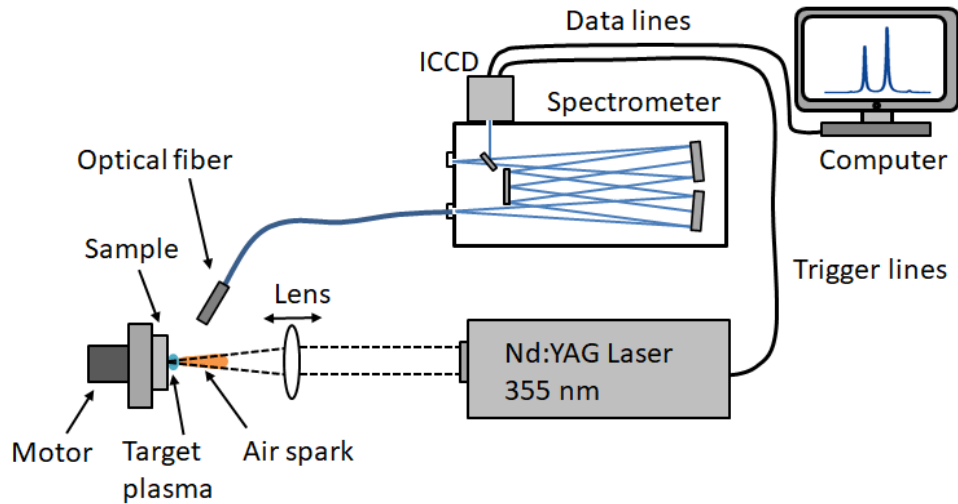


Fig. 1. Schematic diagram of the experimental arrangement.

3. Results and discussions

Before adjusting the sample position on the experimental setup, we need to determine the lens' focal point's location. It was determined based on where the air spark appears when we set the incident laser energy close to the breakdown threshold value. The measured breakdown threshold energy in this experiment was around 1.5 mJ, corresponding to a laser irradiance of 0.5×10^{11} W/cm². Figure 2(a) shows the location of the air spark when we set the incident laser energy to 60 mJ. The red arrow in Fig. 2(a) indicated the lens' focal point location. As seen in Fig. 2(a), the initial breakdown of the air spark moves away from the focal point toward the laser's direction. This shift occurs because the breakdown threshold can be reached earlier at a location before the focal point for higher laser energy, as reported by Chen et al. [35]. It should also be noted that, apart from shifting the air spark's position, higher laser energy will also elongate the air spark.

When we set the laser energy to 60 mJ and place the focal point of the lens on the sample surface, two separate plasmas, namely the target plasma and the air spark, appear simultaneously, as shown in Fig. 2(b). The air spark appears a few mm before the focal point of the lens. At the same time, target plasma appears on the sample's surface. The target plasma can be formed because, under this experimental condition, we found that 50% of the incident laser energy could pass through the air spark. We got this value by measuring the laser energy that passes through the air spark without the presence of the sample and comparing it with the incident laser energy. Therefore when we set the sample surface at the lens' focal point, 50% of the incident laser energy that passes through the air spark can ablate the target and generate the plasma. With time, this target plasma will expand, and as can be observed in Fig. 2(b), its outer shell will interact

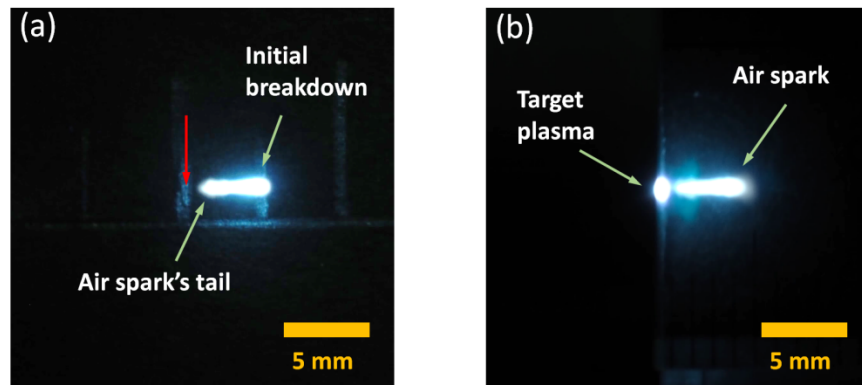


Fig. 2. a) Photograph of the air spark when the sample surface is far away from the lens' focal point. The incident laser energy was set at 60 mJ. The red arrow in the figures indicate the position of lens' focal point. b) Photograph of the air spark and the target plasma when the sample surface was set at the lens' focal point. The incident laser energy was set at 60 mJ.

with the surrounding air molecules. During interaction with the air molecules, the atoms in the target plasma periphery can efficiently dissipate their energy to the large number of available rotational energy states in the air molecules, as explained by Urbina et al. [21]. As a result, the outer shell of the target plasma will be populated by cold ground-state atoms. This condition generates inhomogeneity in the target plasma, and as a consequence, the self-reversal effect will show up in the emission lines, especially for those which have transitioned close to the ground state, as depicted in Fig. 3. Figure 3 shows the time-resolved spectra of the aluminum resonance lines, i.e., the Al I 394.40 nm and Al I 396.15 nm when we set the lens' focal point on the sample surface. The inset of Fig. 3(b) shows the photograph of the resulting plasma. We can infer the appearance of a self-reversal effect in the plasma from a narrow dip on the center of the emission lines. In this configuration, the air spark in front of the target plasma does not contribute much to suppressing the self-reversal effect because of the lack of interaction with the target plasma.

To increase the interaction between the target plasma and the air spark, we shifted the position of the air spark by moving the lens' focal point around 1 mm inside the sample surface. The inset of Fig. 4 shows the photograph of the resulting plasma, showing the interaction between the air spark's tail and the target plasma. In this configuration, the atoms in the target plasma periphery can be excited through the collision with the atomic and ionic species from the air spark. Besides that, the presence of an air spark in front of the target plasma will also slow down the cooling process because, in the air spark, the air molecules have been dissociated into their constituents, which makes them less efficient in dissipating the energy of the target atoms residing in the plasma periphery. Consequently, the number of ground-state atoms will decrease, and the target plasma will become more homogeneous. The plasma homogeneity can be inferred from the time-resolved spectra in Fig. 4, where no apparent self-reversal effect was observed at the Al I 394.40 nm and Al I 396.15 nm emission lines.

However, the self-reversal effect becomes evident when we shift the air spark position further within the target plasma. The inset of Fig. 5. shows the photograph of the resulting plasma when we move the lens' focal point to 2 mm below the sample's surface. In this condition, the air spark was involved in the ablation process of the sample, creating a high-density target plasma. Besides, since the air spark has been moved further within the target plasma, only a small part remains near its outer layer. Thus, the number of atomic or ionic species from the air spark which can collide with the atoms in the target plasma periphery gets reduced. This condition increases

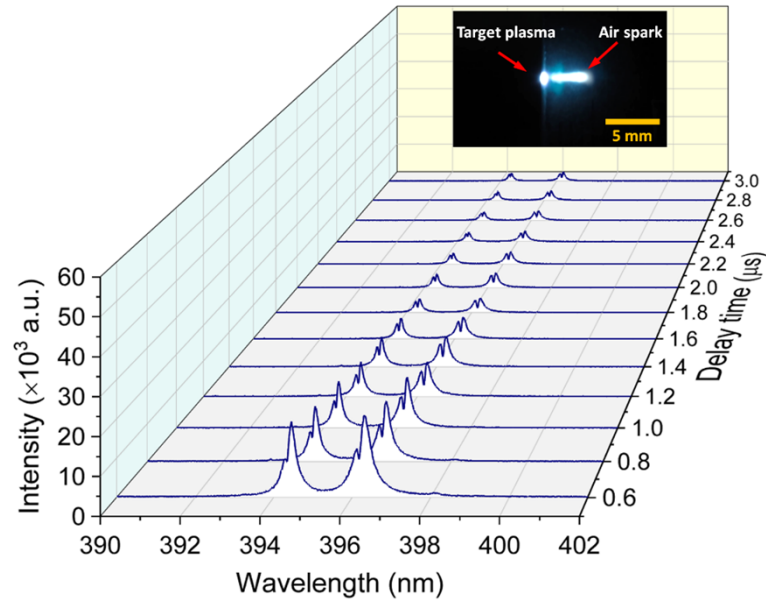


Fig. 3. Time-resolved spectra of the Al I 394.40 nm and Al I 396.15 nm when the position of lens' focal point was set at the sample surface. The gate width of the ICCD was set at 200 ns. Inset in the figure shows the time-integrated photograph of the resulted plasma. The incident laser energy was set at 60 mJ.

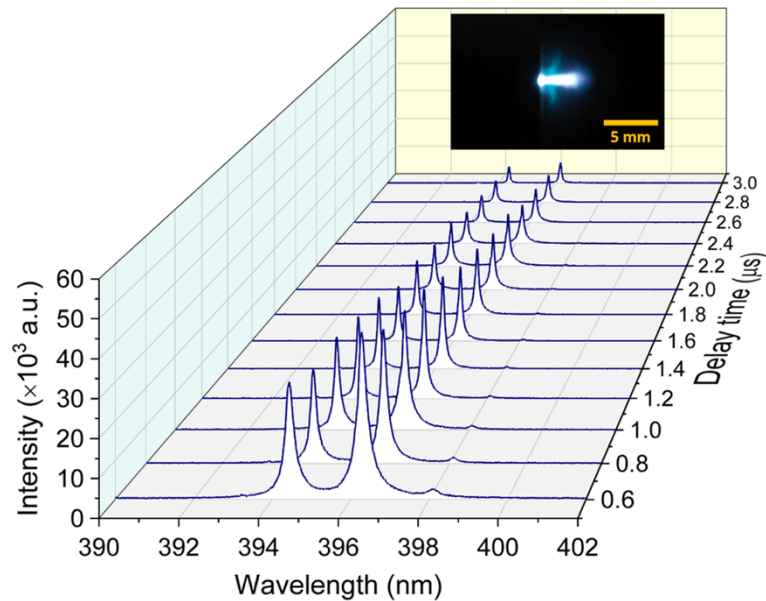


Fig. 4. Time-resolved spectra of the Al I 394.40 nm and Al I 396.15 nm when the position of lens' focal point was set 1 mm below the sample surface. The gate width of the ICCD was set at 200 ns. Inset in the figure shows the photograph of the resulted plasma. The incident laser energy was set at 60 mJ.

the collision probability between the atoms in the outer target plasma with the air molecules and makes the outer plasma layer populated by cold ground-state atoms. Figure 5 shows the time-resolved spectra of the Al I 394.40 nm and Al I 396.15 nm emission lines obtained in this condition. A noticeable dip in the spectral lines indicates the presence of inhomogeneity in the plasma.

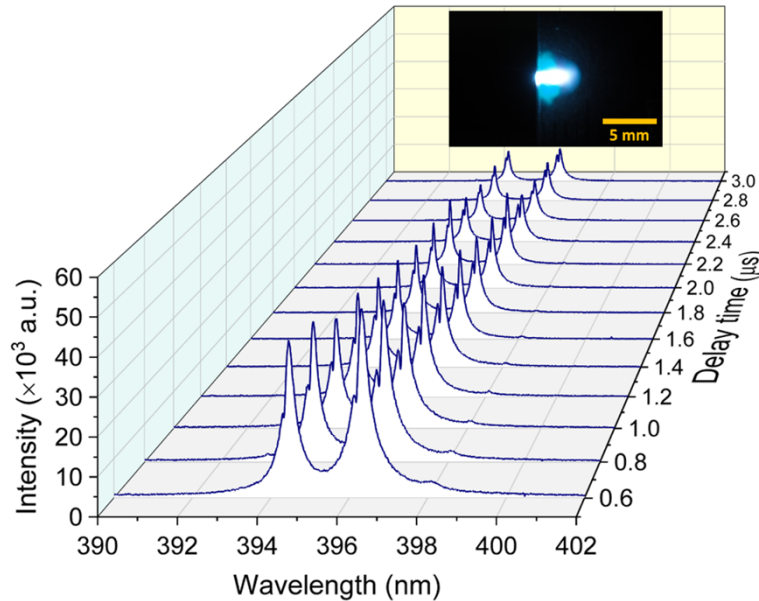


Fig. 5. Time-resolved spectra of the Al I 394.40 nm and Al I 396.15 nm when the position of lens' focal point was set 2 mm below the sample surface. The gate width of the ICCD was set at 200 ns. Inset in the figure shows the photograph of the resulted plasma. The incident laser energy was set at 60 mJ.

Figure 6 shows the resulting time-resolved spectrum when the lens focal point was moved deeper beneath the sample surface, around 3 mm. The inset in Fig. 6 shows the resulting plasma photograph. The spectrum reveals a deeper dip in the emission lines of Al I 394.40 nm and Al I 396.15 nm, a signature of self-reversal arising from the strong plasma's inhomogeneity. In this condition, almost all the incident laser energy was used to ablate the sample. Therefore, the target plasma's density will be higher than in the previous situation, as seen in Fig. 7. Figure 7 displays the calculated temporal electron density derived using the optically thin Al II 281.62 nm ($3s4s^1S - 3s3p^1P$) line [11] when the lens' focal point was moved to 1 mm, 2 mm, and 3 mm, below the sample surface. We calculated the electron density by using the following equation:

$$n_e = \frac{\Delta\lambda}{2\omega_s} \quad (1)$$

where n_e is the calculated electron density, $\Delta\lambda$ is the full width at half maximum (FWHM) of the Al II 281.62 nm line and ω_s is the half-width Stark parameter of the corresponding line taken from Fleurier et. al. [36]. To get the FWHM of the spectral lines, we fitted the experimental profiles with a Voigt profile. Then, the Lorentzian width of the line used to evaluate electron density was acquired by a numerical deconvolution of the Voigt profile using the instrumental profile. The instrumental profile broadening was measured using spectral lines emitted from a low-pressure argon mercury lamp in the wavelength region of interest. In addition to the higher plasma density, in this condition, the air spark has also been moved inside the target plasma like

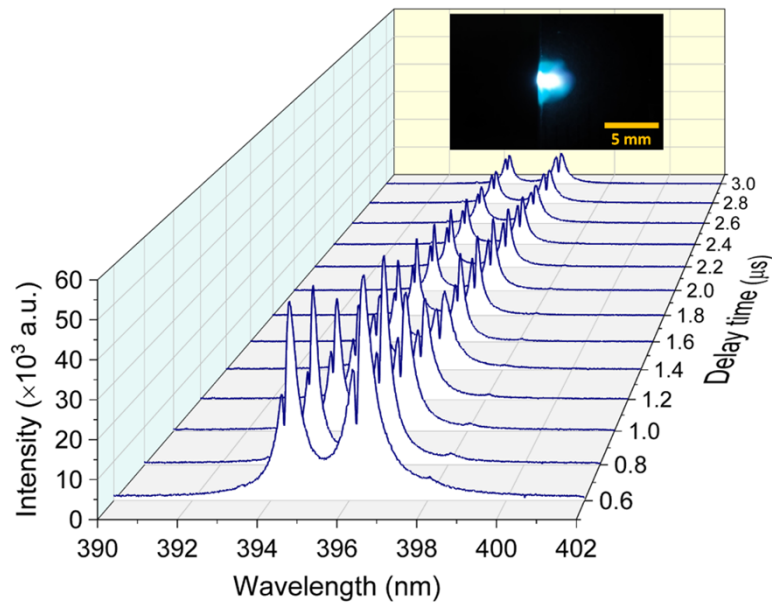


Fig. 6. Time-resolved spectra of the Al I 394.40 nm and Al I 396.15 nm when the position of lens' focal point was set 3 mm below the sample surface. The gate width of the ICCD was set at 200 ns. Inset in the figure shows the photograph of the resulted plasma. The incident laser energy was set at 60 mJ.

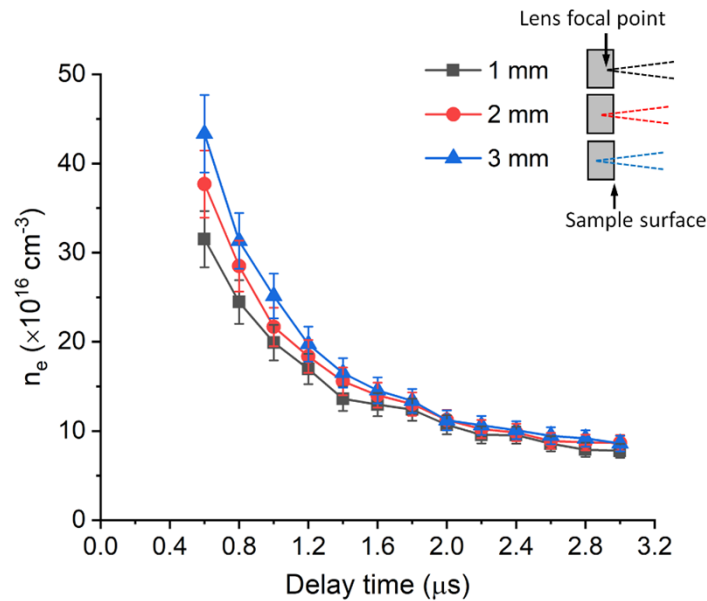


Fig. 7. Temporal variation of electron density derived from Al II 281.62 nm line when the lens' focal point was set at 1 mm, 2 mm, and 3 mm below the sample surface and the incident laser energy was set at 60 mJ. The error of the electron density is 10%.

in the previous case, so it does not contribute to the excitation of the ground-state atoms at the periphery of the target plasma. Consequently, the aluminum atoms at the target plasma periphery

can easily interact with the air molecules, which explains the appearance of a strong self-reversal effect manifesting as a deeper dip in the emission lines.

From these results, we found that the number of cold ground-state atoms in the periphery of the target plasma can be suppressed when the air spark's tail was positioned between the sample surface and the outer layer of the target plasma. In this condition, the N and O atoms in the air spark can excite the ground state atoms in the target plasma by collisions, resulting in the self-reversal free of the emission lines. From the self-reversal free of Al I 394.40 nm and Al I 396.15 nm emission lines, we can easily evaluate the self-absorption coefficient (SA) from these lines by using the following equation [11]:

$$SA = \left(\frac{\Delta\lambda^{line}}{2\omega_s^{line} n_e^{281.62\text{ nm}}} \right)^{1/\alpha} = \left(\frac{n_e^{line}}{n_e^{281.62\text{ nm}}} \right)^{1/\alpha} \quad (2)$$

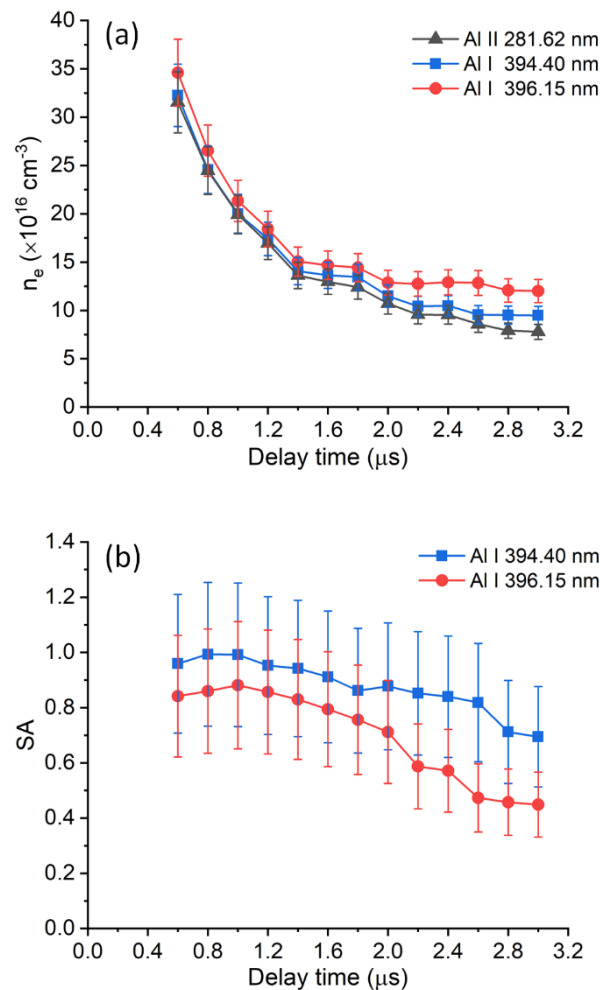


Fig. 8. a) Temporal variation of electron density derived from Al II 281.62 nm, Al I 394.40 nm and Al I 396.15 nm lines when the lens' focal point was set at 1 mm and the laser energy was set at 60 mJ. The error of the electron density is 10%. b) Self-absorption coefficient (SA) for Al I 394.40 nm and Al I 396.15 nm. The errors of the SA for both lines are about 30%.

where $\Delta\lambda^{line}$ is the FWHM of a measured spectral line, $n_e^{281.62\text{ nm}}$ is the electron density calculated from the optically thin line Al II 281.62 nm [11], ω_s^{line} is the half-width Stark parameter for the corresponding line taken from Fleurier et. al [36], and α is the empirically derived constant that is equal to -0.54 [11]. Figure 8(a) shows the calculation result of temporal electron density derived using Al I 281.62 nm, Al I 394.40 nm, and Al I 396.15 nm emission lines obtained when we set the lens' focal point 1 mm below the sample surface. The calculated SA for Al I 394.40 nm and Al I 396.15 nm was presented in Fig. 8(b). SA reaches unity when the self-absorption effects are negligible and decreases to the limit of zero when the self-absorption effects are severe [11].

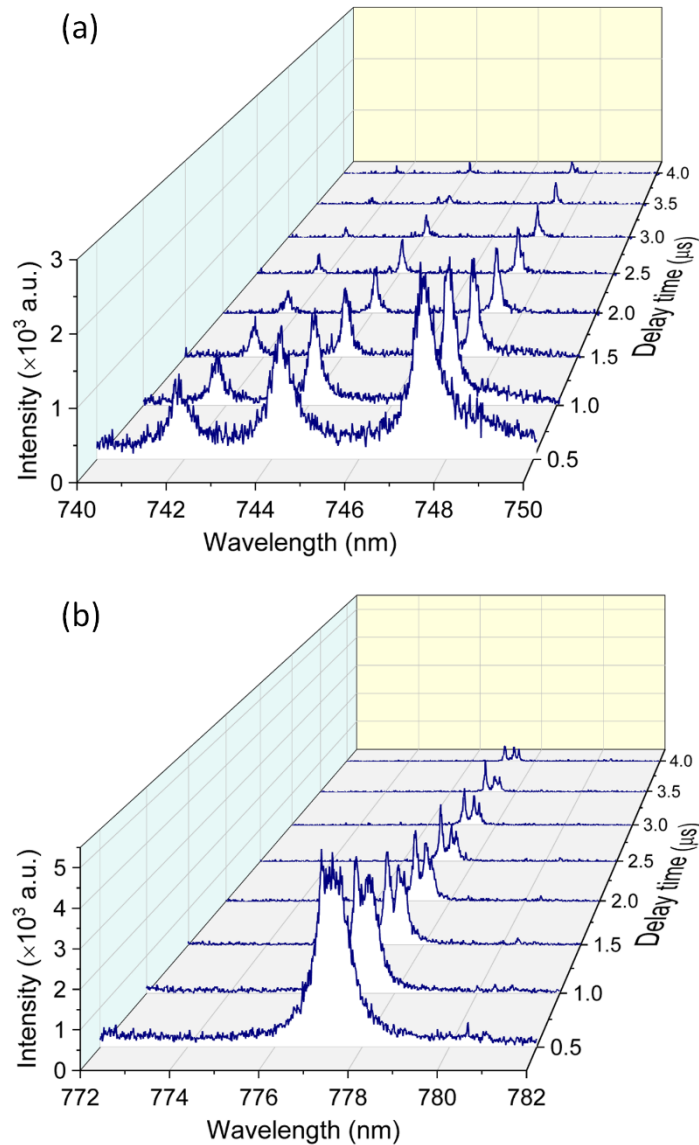


Fig. 9. a) Time-resolved spectra of a) Ni I 742.4 nm, Ni I 744.2 nm and Ni I 746.8 nm and b) time resolved spectra of O I 777.2 nm, O I 777.4, and O I 777.5 nm when the position of lens' focal point was set 1 mm below the sample surface and the laser energy was set at 60 mJ. The gate width of the ICCD was set at 500 ns.

From Fig. 8(b), we can see that the SA of Al I 396.15 nm is always lower than Al I 394.40 nm meaning the Al I 396.15 nm line has a high degree of self-absorption compared to Al I 394.40 nm line. This condition can be attributed to Al I 396.15 nm's higher transition probability than Al I 394.40 nm. By looking at the temporal evolution of the SA values shown in Fig. 8(b), we found that the best time window to perform a quantitative analysis using the proposed configuration was 0.8 μ s -1.2 μ s, i.e., when the self-absorption effect was minimum. After 1.2 μ s, the SA value keeps decreasing. This reduction can be caused by reducing the number of N and O atoms in the air spark due to the cooling process. Figures 9 (a) and (b) show the temporal profile of N and O spectrums, respectively. As shown in the figures, the emission intensity of N and O reduced with time, confirming the reduction of the number of N and O atoms in the plasma. Lastly, we calculate the spectral lines' relative standard deviation (RSD) to evaluate spectral stability. The RSD was calculated from 10 spectra; each spectrum had an average of 10 laser shots. The RSD for the Al I 394.40 nm and Al I 396.15 nm lines at a gate delay of 1 μ s was calculated to be 3.3% and 5.0%, respectively.

4. Conclusions

In summary, utilizing an air spark, we have demonstrated a simple method for suppressing the self-reversal effect in single-pulse UV LIBS in atmospheric pressure. We have shown that by appropriately adjusting the lens' focal point position, we can simultaneously generate the air spark and target plasma. The homogeneity of the target plasma improved when the air spark's tail was positioned between the sample surface and the target plasma periphery. By employing this technique, we successfully obtain the emission lines of high-concentration aluminum that are free from self-reversal at 394.40 nm and 396.15 nm. These results suggest that the proposed approach can help suppress the self-reversal effect in nanosecond UV LIBS and improve the spectral quality of resonance lines of nanosecond UV LIBS.

Funding. Kementerian Pendidikan, Kebudayaan, Riset dan Teknologi Indonesia (020/UKKW/LPPM-FTIK/PDUPT/VI/2022, 155/E5/PG.02.00.PT/2022, 425/LL3/AK.04/2022); Third World Academy of Sciences (TWAS) (060150 RG/PHYS/AS/UNESCO FR:3240144882).

Acknowledgments. All the authors would like to thank the Maju Makmur Mandiri Research Center for facilitating this research.

Disclosures. The authors declare no conflicts of interest.

Data availability. Data underlying the results presented in this paper are not publicly available at this time but may be obtained from the authors upon reasonable request.

References

1. M. Gaft, E. Dvir, H. Modiano, and U. Schone, "Laser Induced Breakdown Spectroscopy machine for online ash analyses in coal," *Spectrochim. Acta, Part B* **63**(10), 1177–1182 (2008).
2. A. F. M. Y. Haider, M. Parvin, Z. H. Khan, and M. Wahadoszamen, "Highly Sensitive Detection of Lead in Aqueous Solution using Laser-Induced Breakdown Spectroscopy Coupled with Adsorption Technique," *J. Appl. Spectrosc.* **87**(6), 1163–1170 (2021).
3. R. Harmon, C. Lawley, J. Watts, C. Harraden, A. Somers, and R. Hark, "Laser-Induced Breakdown Spectroscopy—An Emerging Analytical Tool for Mineral Exploration," *Minerals* **9**(12), 718 (2019).
4. A. K. Knight, N. L. Scherbarth, D. A. Cremers, and M. J. Ferris, "Characterization of Laser-Induced Breakdown Spectroscopy (LIBS) for Application to Space Exploration," *Appl. Spectrosc.* **54**(3), 331–340 (2000).
5. R. Hedwig, K. Lahna, R. Idroes, I. Karnadi, I. Tantra, J. Iqbal, D. Kwaria, D. P. Kurniawan, K. H. Kurniawan, M. O. Tjia, and K. Kagawa, "Food analysis employing high energy nanosecond laser and low pressure He ambient gas," *Microchem. J.* **147**, 356–364 (2019).
6. S. N. Abdulmajid, M. Pardede, H. Suyanto, M. Ramli, K. Lahna, A. M. Marpaung, R. Hedwig, Z. S. Lie, D. P. Kurniawan, K. H. Kurniawan, T. J. Lie, N. Idris, M. O. Tjia, and K. Kagawa, "Evidence of feasible hardness test on Mars using ratio of ionic/neutral emission intensities measured with laser-induced breakdown spectroscopy in low pressure CO₂ ambient gas," *J. Appl. Phys. (Melville, NY, U. S.)* **119**(16), 163304 (2016).
7. A. Lang, D. Engelberg, N. T. Smith, D. Trivedi, O. Horsfall, A. Banford, P. A. Martin, P. Coffey, W. R. Bower, C. Walther, M. Weiß, H. Bosco, A. Jenkins, and G. T. W. Law, "Analysis of contaminated nuclear plant steel by laser-induced breakdown spectroscopy," *J. Hazard. Mater.* **345**, 114–122 (2018).

8. M. Kuzuya and O. Mikami, "Effect of argon pressure on spectral emission of a plasma produced by a laser microprobe," *J. Anal. At. Spectrom.* **7**(3), 493–497 (1992).
9. H. Amamou, A. Bois, B. Ferhat, R. Redon, B. Rossetto, and P. Matheron, "Correction of self-absorption spectral line and ratios of transition probabilities for homogeneous and LTE plasma," *J. Quant. Spectrosc. Radiat. Transfer* **75**(6), 747–763 (2002).
10. J. A. Aguilera, J. Bengoechea, and C. Aragón, "Curves of growth of spectral lines emitted by a laser-induced plasma: influence of the temporal evolution and spatial inhomogeneity of the plasma," *Spectrochim. Acta, Part B* **58**(2), 221–237 (2003).
11. A. M. El Sherbini, T. M. El Sherbini, H. Hegazy, G. Cristoforetti, S. Legnaioli, V. Palleschi, L. Pardini, A. Salvetti, and E. Tognoni, "Evaluation of self-absorption coefficients of aluminum emission lines in laser-induced breakdown spectroscopy measurements," *Spectrochim. Acta, Part B* **60**(12), 1573–1579 (2005).
12. F. Bredice, F. O. Borges, H. Sobral, M. Villagran-Muniz, H. O. Di Rocco, G. Cristoforetti, S. Legnaioli, V. Palleschi, L. Pardini, A. Salvetti, and E. Tognoni, "Evaluation of self-absorption of manganese emission lines in Laser Induced Breakdown Spectroscopy measurements," *Spectrochim. Acta, Part B* **61**(12), 1294–1303 (2006).
13. F. Rezaei and S. H. Tavassoli, "Utilizing the ratio and the summation of two spectral lines for estimation of optical depth: Focus on thick plasmas," *Spectrochim. Acta, Part B* **125**, 25–30 (2016).
14. Z. Q. Hao, L. Liu, M. Shen, X. Y. Yang, K. H. Li, L. B. Guo, X. Y. Li, Y. F. Lu, and X. Y. Zeng, "Investigation on self-absorption at reduced air pressure in quantitative analysis using laser-induced breakdown spectroscopy," *Opt. Express* **24**(23), 26521–26528 (2016).
15. Y. Tang, S. Ma, Y. Chu, T. Wu, Y. Ma, Z. Hu, L. Guo, X. Zeng, J. Duan, and Y. Lu, "Investigation of the self-absorption effect using time-resolved laser-induced breakdown spectroscopy," *Opt. Express* **27**(4), 4261–4270 (2019).
16. R. Yi, L. Guo, C. Li, X. Yang, J. Li, X. Li, X. Zeng, and Y. Lu, "Investigation of the self-absorption effect using spatially resolved laser-induced breakdown spectroscopy," *J. Anal. At. Spectrom.* **31**(4), 961–967 (2016).
17. M. Kuzuya and H. Aranami, "Analysis of a high-concentration copper in metal alloys by emission spectroscopy of a laser-produced plasma in air at atmospheric pressure," *Spectrochim. Acta, Part B* **55**(9), 1423–1430 (2000).
18. R. Hai, Z. He, X. Yu, L. Sun, D. Wu, and H. Ding, "Comparative study on self-absorption of laser-induced tungsten plasma in air and in argon," *Opt. Express* **27**(3), 2509–2520 (2019).
19. A. M. E. L. Sherbini, A. H. E. L. Farash, T. M. E. L. Sherbini, and C. G. Parigger, "Opacity Corrections for Resonance Silver Lines in Nano-Material Laser-Induced Plasma," *Atoms* **7**(3), 73 (2019).
20. H. Cui, Y. Tang, S. Ma, Y. Ma, D. Zhang, Z. Hu, Z. Wang, and L. Guo, "Influence of laser wavelength on self-absorption effect in laser-induced breakdown spectroscopy," *Optik (Munich, Ger.)* **204**, 164144 (2020).
21. I. Urbina, F. Bredice, C. Sanchez-Aké, M. Villagrán-Muniz, and V. Palleschi, "Temporal analysis of self-reversed Ag I resonant lines in LIBS experiment at different laser pulse energy and in different surrounding media," *Spectrochim. Acta, Part B* **195**, 106489 (2022).
22. M. Pardede, I. Karnadi, Z. S. Lie, E. Jobiliong, I. Tanra, R. Hedwig, A. M. Marpaung, H. Suyanto, M. M. Suliyanti, D. Kwaria, T. J. Lie, K. H. Kurniawan, and K. Kagawa, "Unusual parallel laser irradiation for suppressing self-absorption in single pulse laser-induced breakdown spectroscopy," *Opt. Express* **29**(14), 22593–22602 (2021).
23. A. M. Marpaung, E. Harefa, and M. Pardede, *et al.*, "Simple defocus laser irradiation to suppress self-absorption in laser-induced breakdown spectroscopy (LIBS)," *Heliyon* **8**(8), e10057 (2022).
24. J. Viljanen, Z. Sun, and Z. T. Alwahabi, "Microwave assisted laser-induced breakdown spectroscopy at ambient conditions," *Spectrochim. Acta, Part B* **118**, 29–36 (2016).
25. J.-M. Li, L.-B. Guo, C.-M. Li, N. Zhao, X.-Y. Yang, Z.-Q. Hao, X.-Y. Li, X.-Y. Zeng, and Y.-F. Lu, "Self-absorption reduction in laser-induced breakdown spectroscopy using laser-stimulated absorption," *Opt. Lett.* **40**(22), 5224–5226 (2015).
26. J. Li, Y. Tang, Z. Hao, N. Zhao, X. Yang, H. Yu, L. Guo, X. Li, X. Zeng, and Y. Lu, "Evaluation of the self-absorption reduction of minor elements in laser-induced breakdown spectroscopy assisted with laser-stimulated absorption," *J. Anal. At. Spectrom.* **32**(11), 2189–2193 (2017).
27. Y. Tang, J. Li, Z. Hao, S. Tang, Z. Zhu, L. Guo, X. Li, X. Zeng, J. Duan, and Y. Lu, "Multielemental self-absorption reduction in laser-induced breakdown spectroscopy by using microwave-assisted excitation," *Opt. Express* **26**(9), 12121–12130 (2018).
28. Y. Tang, L. Guo, J. Li, S. Tang, Z. Zhu, S. Ma, X. Li, X. Zeng, J. Duan, and Y. Lu, "Investigation on self-absorption reduction in laser-induced breakdown spectroscopy assisted with spatially selective laser-stimulated absorption," *J. Anal. At. Spectrom.* **33**(10), 1683–1688 (2018).
29. Q. Wang, A. Chen, Y. Liu, X. Gao, and M. Jin, "Reduction of self-absorption in femtosecond laser-induced breakdown spectroscopy using spark discharge," *Phys. Plasmas* **28**(8), 083301 (2021).
30. R. Hedwig, I. Tanra, I. Karnadi, M. Pardede, A. M. Marpaung, Z. S. Lie, K. H. Kurniawan, M. M. Suliyanti, T. J. Lie, and K. Kagawa, "Suppression of self-absorption effect in laser-induced breakdown spectroscopy by employing a Penning-like energy transfer process in helium ambient gas," *Opt. Express* **28**(7), 9259–9268 (2020).
31. I. Karnadi, M. Pardede, I. Tanra, R. Hedwig, A. M. Marpaung, Z. S. Lie, E. Jobiliong, D. Kwaria, M. M. Suliyanti, M. Ramli, K. Lahna, T. J. Lie, H. Suyanto, K. H. Kurniawan, and K. Kagawa, "Suppression of self-absorption in laser-induced breakdown spectroscopy using a double pulse orthogonal configuration to create vacuum-like conditions in atmospheric air pressure," *Sci. Rep.* **10**(1), 13278 (2020).

32. W. Wang, L. Sun, P. Zhang, L. Zheng, and L. Qi, "Reducing self-absorption effect by double-pulse combination in laser-induced breakdown spectroscopy," *Microchem. J.* **172**, 106964 (2022).
33. F. Rezaei, G. Cristoforetti, E. Tognoni, S. Legnaioli, V. Palleschi, and A. Safi, "A review of the current analytical approaches for evaluating, compensating and exploiting self-absorption in Laser Induced Breakdown Spectroscopy," *Spectrochim. Acta, Part B* **169**, 105878 (2020).
34. Q. Ma, V. Motto-Ros, F. Laye, J. Yu, W. Lei, X. Bai, L. Zheng, and H. Zeng, "Ultraviolet versus infrared: Effects of ablation laser wavelength on the expansion of laser-induced plasma into one-atmosphere argon gas," *J. Appl. Phys. (Melville, NY, U. S.)* **111**(5), 053301 (2012).
35. Y.-L. Chen, J. W. Lewis, and C. Parigger, "Spatial and temporal profiles of pulsed laser-induced air plasma emissions," *J. Quant. Spectrosc. Radiat. Transfer* **67**(2), 91–103 (2000).
36. C. Fleurier, S. Sahal-Brechot, and J. Chapelle, "Stark profiles of Al I and Al II lines," *J. Phys. B: At. Mol. Phys.* **10**(17), 3435–3441 (1977).